NASA Technical Memorandum 81668

Factors Which Influence the Behavior of Turbofan Forced Mixer Nozzles

B. H. Anderson and L. A. Povinelli
Lewis Research Center
Cleveland, Ohio

Prepared for the
Nineteenth Aerospace Sciences Meeting
sponsored by the American Institute of
Aeronautics and Astronautics
St. Louis, Missouri, January 12-15, 1981

NASA

FACTORS WHICH INFLUENCE THE BEHAVIOR OF TURBOFAN FORCED MIXER NOZZLES

by B. H. Anderson* and L. A. Povinelli**
National Aeronautics and Space Administration
Lewis Research Center
Cleveland, Ohio

SUMMARY

A finite difference procedure was used to compute the mixing for three experimentally tested mixer geometries. Good agreement was obtained between analysis and experiment when the mechanisms responsible for secondary flow generation were properly modeled. Vorticity generation due to flow turning and vorticity generated within the centerbody-lobe passage were found to be important. Results are presented for two different temperature ratios between fan and core streams and for two different free-stream turbulence levels. It was concluded that the dominant mechanisms in turbofan mixers is associated with the secondary flows arising within the lobe region and their development within the mixing section.

E-689

INTRODUCTION

Significant performance gains are achievable in turbofan engines by mixing the hot core stream with the cooler fan stream prior to expansion through the exhaust nozzle. The amount of performance gain depends on the balance between the degree of mixing of the hot and cold streams, and the pressure losses incurred during the mixing process. The lobe mixer has been the most successful device that has been used to promote mixing. To date, the performance of lobe mixers has been determined almost entirely through experimentation.[1,2,3] These experiments were sufficient to determine the relative merits of one lobe configuration over another. However, in the absence of any clear understanding of the mixing process, conclusions reached with one series of tests could not be generalized to the next generation of mixer nozzles. Fluid flow analysis for the design of turbofan mixer nozzles was first published by Birch, Paynter, Spaling, and Tatchell[4] and showed encouraging results. However, the role of various aerodynamic processes which take place within the mixer nozzles was clearly still not understood. It was first suggested in the Lewis Aeropropulsion 1979 Conference[5] and later by Povinelli, Anderson, and Gerstenmaier[6] that convective forces arising from pressure driven secondary flows play a far more important role in the mixing processes than first anticipated. These convective forces arise due to secondary flows at entry, which are sustained and amplified in the mixer passage by transverse pressure gradients that deflect the mean flow.

---

*Head, Aerodynamics Analysis Section; Member, AIAA.
**Aerospace Engineer; Aerodynamics Analysis Section, Associate Fellow, AIAA.

These conclusions were based on the computations obtained with the viscous marching procedure developed by Kriskovsky, Briley, and McDonald.[7,8]. Subsequently, LDV measurements performed at UTRC under Lewis sponsorship, clearly demonstrated the presence of strong radial and some tangential flows at the lobe exit plane (ref. 9). Concurrently, flow surveys at Lewis, revealed radial temperature profiles whose particular patterns could be explained by the presence of radial and tangential flows within the mixing duct (ref. 6). In addition, flow angularity data were obtained which revealed strong radial flows at the lobe exit plane. Computations were then performed using a representative or generic secondary flow field as a starting condition for the computer program (ref. 10). Use of the generic flow field simplified the task of obtaining data for the initial starting profile and led to good agreement between experiment and computation for a typical model mixer. However, application of the analysis to several other geometries suggested that not all of the flow phenomena were accounted for in the starting profiles. It is postulated that other basic geometry dependent flow structures exist at the mixer entry which have an influence on the flow development. These include hot flow under the fan trough or additional vortex structures. Specifically, the objective of the present study was to further define possible vortex mechanisms occurring in the mixing passage and to demonstrate the ability of a 3D viscous computer analysis to calculate the flow in a variety of turbofan mixers.

ANALYSIS

The calculational procedure used in this study of forced mixer nozzle flow fields is an application of the approach developed by Briley, McDonald, and Kreskovsky[7,8] and is designated PEPSIM. The procedure is based on the decomposition of the velocity field into primary and secondary flow velocities. Equations governing the streamwise development of the primary and secondary flow velocity fields are solved by an efficient algorithm using both block and scalar ADI methods. Although the governing equations are solved by a forward marching method, elliptic effects due to curvature and area change are accounted for a-priori through the imposed pressure gradients determined from a potential flow solution for the geometry in question. Since the primary concern in the lobe mixer problem is thermal mixing of the fan and core streams to achieve thrust augmentation, an energy equation is introducted.

For turbulent flows, the turbulent viscosity which appears in the governing equations must be specified. Two types of turbulent models are used in PEPSIM to determine turbulent viscosity; a two-equation k-ε turbulence model as presented by Launder and Spaulding[11] and a wake-turbulence model. In this paper, only the results obtained with the wake turbulence model are presented. In the wake-turbulence model, the assumption is made that the turbulent velocity and length scales are frozen at their initial value. Thus, the turbulent viscosity is proportional to density.

Specification of the initial (inflow) conditions for a lobe mixer calculation in PEPSIM may be performed either by specifying the initial values of the velocity and temperature field or by using an automated procedure which constructs the initial velocity and temperature fields parametrically. In either case it is unlikely that the specified velocity field would be compatible with the continuity equations. Therefore, this velocity field is modified in a way that makes it compatible with the continuity equation while at the same time maintaining the initial secondary flow vor-

ticity unaltered. The streamwise momentum equation is solved to obtain approximate values for the streamwise velocity gradients. The secondary flow vorticity is computed from the specified velocity field. A scalar potential is then constructed and solved yielding the irrotational components of the secondary flow which balance the streamwise velocity gradient in the continuity equation. Finally, a vector potential is constructed using the initial secondary flow vorticity and solved yielding the irrotational components of the secondary flow. Due to the nature of the vector potential these velocity components do not effect the continuity balance obtained from the scalar potential. The resulting velocity field is compatible with the continuity equation to first order in the marching direction.

EXPERIMENTAL APPARATUS

The test apparatus used has been described in a previous paper[6] and consisted of two basic parts: a fixed upstream model section and a rotating shroud (fig. 1). The upstream section simulated the flow path through a typical high by-pass turbofan engine. A cross-section of the model is shown in figure 2(a). Heated air was supplied to the core passage and flowed through the lobe section. Unheated air was supplied to the fan passage and flowed around the lobe section which was interchangeable. In this paper, the results obtained with three mixer sections are presented. The longitudinal contours of the three mixers are shown in figure 2(b). Configurations A, B, and C has a penetration (lobe tip radius/shroud radius) of 0.822, 0.776, and 0.721 and the circumferential spacing ratio (core included angle/fan included angle) of 0.5, 1.0, and 1.36. The ratio of the shroud length to the inside shroud diameater (at the lob exit plane) was 0.71.

Total pressure and temperature measurements were made upstream in both the fan and core flows. Instrumentation rakes were also mounted in the rotating shroud for probing the mixer flow field (see fig. 2). Total temperature rakes were located at five axial stations in the mixing region. The first station was at the lobe exit plane, the second was halfway to the end of the plug, the third was at the end of the plug, the fourth was midway between the plug end and the nozzle exit, and the fifth station was at the nozzle exit plane. The rakes at the lobe and nozzle exit stations as well as the rotating mechanism are shown in figure 1. Total pressures were also measured at the lobe and nozzle exit stations. The temperature data were obtained over a 54-degree segment in 3-degree increments at 14 radial positions. Flow angularity measurements using the fixed probe technique[12] were made at four circumferential locations and at the two axial locations shown in figure 2. The first measuring station was at the lobe exit plane; the second at the end of the centerbody. A photograph of the angularity rakes are shown in figure 3. Each rake has six probes and each probe has three tubes. The center tube is a chambered total pressure probe and the two side (upper and lower) tubes have a 45-degree sweepback. The pressure difference between the two side probes and the indicated total pressure were used along with a calibration curve in order to obtain flow directions (radial and azimutnal). Each probe was individually calibrated in an open jet at a Mach number of 0.45, wherein the radial probe was set at various pitch angles to the flow and the azimuthal probe at various yaw angles. The indicated total pressure and the differences in side tube (upper-lower) pressures were used to establish a calibration.

Wall static pressure measurements completed the information needed to compute a resultant velocity. The resultant velocity was then used with the radial and azimuthal flow angles to compute the three velocity components.

The fan and core streams were operated with a total pressure ratio of one and a total temperature ratio of (fan/core) of 0.74 or 0.4. The Mach number of the fan and core streams at the mixing plane (lobe exit) was approximately 0.45 and the by-pass ratio was about 4.

COMPUTATIONAL PROCEDURE

A. Computational Mesh

In this section, specific details arising from the application of the foregoing analysis to the turbofan mixer configuration described earlier is given. The cross-section of this mixer geometry is presented in figure 4. The area immediately downstream of the nozzle plug tip is faired in with an assumed streamline to model the separated flow region expected in this mixer nozzle. Since the flow area excluded from consideration is small, this treatment is not believed to introduce significant error. The curvilinear coordinate system shown in figure 4 was constructed to fit the flow passage boundaries and has 21 streamwise nodal points, 40 radial nodes and 11 azimuthal modes. In planes of constant azimuth, orthogonal streamlines and velocity potential lines were constructed from a two-dimensional plane incompressible analysis.[13] This x-y coordinate system was then rotated about the mixer axis to form the axisymmetric coordinate system. Five reference stations are identified in figure 4 and these correspond to the five experimental survey stations mentioned in the previous section. These are labeled 1, 8, 13, 17, and 21 and correspond to the computation nodal point nearest to the probing stations. Station number 1 corresponds to the lobe exit station while station number 21 is the mixer exit station.

Although the mixer geometry is axisymmetric, the flow is three dimensional due to the aximuthal variation of the hot and cold streams. However, due to observed symmetry, only a 1/2 lobed pie-shaped segment of the transverse coordinate surface was considered. The shape of this segment and the extent to typical hot and cold streams at the lobe exit station is shown in figure 5. A comparison between the computational and experimental lobe shape are also shown in figure 5.

B. Flow Angularity Measurements

The three velocity components near the exit popane of the lobes were measured using the flow angularity probes described in the Apparatus section. The flow angularity data were obtained in order to provide information about the mixer inflow conditions The data were measured in a plane parallel to the exit plane of the lobes (see fig. 2). Data were obtained at six radial locations and four circumferential positions within the measurement domain shown in figure 6 for the 12B and 12C lobe geometries. The vectors shown in figure 6 are the resultant of the measured radial and azimuthal velocities in a plane transverse to the mean flow. Strong radial flows are evident with outflow in the core and inflow in the fan regions. Data of this type were discussed previously in reference 6 and it was suggested that a vortex-type flow was present at the fan-core interfacial regions. In reference 6, the flow angularity dat was "enriched," using a four-point linear interpolation scheme. The enrichment was carried out in order to obtain a

more complete representation of the secondary flow structure at the lobe exit plane.

Computations, using the generic starting data yielded good agreement with the data for configuration 12B (see ref. 10). However, comparisons between analyses and experimental data for configurations 12A and 12C indicated that perhaps the initial starting conditions for the computer code were not correct. The comparisons prompted an evaluation of the mechanisms responsible for the generation of secondary flows.

C. Secondary Flow Generation

As mentioned previously in reference 5, streamwise vorticity is generated at the entrance to the mixer and sustained and amplified in the mixer passage by transverse pressure gradients that deflect the mean flow. Three additional mechanisms appear to be responsible for the generation of secondary flow in lobe mixer geometries. The most important one is due to the basic turning of the fan and core streams in oppsite radial directions, as shown in figure 7(a). The secondary flow generation here is basically an inviscid phenomenon and results in outward radial core flow adjacent to inward radial fan flow as shown in figure 7(b). It is believed that this mechanism is properly represented in the starting conditions via the flow angularity data obtained for each lobe geometry. The second mechanism reponsible for secondary flow is due to the interaction of upstream duct boundary layers with the lobes, which in this case represent flow obstructions, as shown conceptually in figure 8. The vorticity within the boundary layers encounters the lobes and vortex filaments wrap around the lobe in a horseshoe-like pattern. A set of vortices are subsequently set up both in the fan troughs and a set in the core flow. However, inspection of the experimental radial and tangential velocities at the lobe exit plane did not indicate that any significant effects were caused by this second mechanism. In addition, the low penetration lobes would tend to minimize the formation of strong horseshoe vortices. See reference 14 for further information. The third mechanism responsible for secondary flows is a passage vortex which occurs as the core flow approaches the lobe exit and encounters the narrow gap between the centerbody and the bottom of the fan trough. As shown in figure 9, the vortex forms as flow washes up around the side of the fan troughs. Tuft photographs taken of the inside surface of the lobes revealed a strong upward radial velocity component near the bottom of the lobe as shown in figure 10. Subsequent turning of the flow in the downstream direction occurs at a slightly larger radial position as indicated by the tufts in figure 10. The behavior of the tufts strongly suggests the presence of a passage vortex. It was decided, therefore, to model the vortex in order to obtain the proper starting conditions for the computer code. In the absence of any measurements of the passage vortex strength, a nominal value of the radial outflow was assumed for the initial computation. Subsequent estimates of the vortex strength were made for the final computations which are presented in this paper.

It should be noted that the computational model, shown in figure 5, does not include a hot core layer between the centerbody and the bottom of the fan trough. Additional grid resolution in the code is required before the effect of this layer on the computations can be assessed.

D. Representation of the Inlet Flow Field

The secondary flow, that is, the flow that is generated transverse to the streamwise direction, is highly complex after passing through the curves lobe section. This highly complex nature of the real flow field procludes numerical simulation of all the large scale and small scale structure simply because this information is not available. However, the large radial velocities of the secondary inflow field can be measured experimentally and simulated. This class of secondary inflow representation is labeled generic flow fields, that is, they attempt to simulate the large scale secondary flow field structure entering the mixer section by a parametric representation, as well as modeling the passage vortices. For comparative purposes, a baseline generic flow field is defined which is the generic flow without passage vortex modeling. The baseline flow was used in earlier results (ref. 10). In contrast to real and generic inflow representations, ideal inflow conditions incoprorate no secondary flows entering the mixer passage. The flow in this case is parallel to the streamwise coordinate of the mesh and was used in the earlier results presented by Povinelli, Anderson, and Gerstenmaier.[6]

A generic representation of the large scale flow transverse to the streamwise direction can be conceived as being composed of basically radial outflow in the core passage and radial inflow in the fan passage (fig. 5). The experimental data for the mixer nozzle 12B configuration under study suggests that the radial velocities in the core and fan lobe passages are 25 and 20 percent, respectively, of the streamwise velocity. For the 12A and 12C geometries, the core flow was 14 percent and the fan flow was 8 percent. The streamwise velocity at each mesh point in the two respective streams was assigned its nondimentional reference value which was then corrected to account for normal pressure gradients at the initial plane as determined from the axisyammetric potential flow. To account for boundary layers on the lobe, plug and shroud surface, the streamwise velocity profiles were further scaled in accordance with an assumed turbulent boundary layer profile and distance from the lobe surface. The temperature field was constructed in the core and fan streams by assuming a total temperature ratio $T_{fan}/T_{core} = 0.74$ and 0.4, which corresponds to the experimental temperature ratios. In addition, an entrance Mach number of 0.45 was assumed.

The initial turbulence quantities were initialized through specification of a length scale and free stream turbulence intensities. These turbulence quantities are assumed to be constant across the shear layer but to vary with distance from the wall. For the calculations presented in this paper, the initial length scale was set at 0.006 of the outer shroud radius and turbulent intensity of both the core and fan streams was set at either 4 or 12 percent.

RESULTS

A. Influence of Secondary Flow Field

12B Mixer

The starting velocity vector field constructed according to the procedure described in the previous section is shown in figure 22 for the 12B mixer. Construction of the secondary velocity vector field was based on average radial secondary flows of 25 and 20 percent of the streamwise core

and fan velocities, coirresponding to the experimental measurements. Although the computational segment included only one half the lobe segment and one half the core passage, the computational results in figure 11 were reflected to represent one lobe and two fan regions. The secondary velocities presented are normal to the streamwise mesh coordinate and are shown only in the region near the plug (centerbody) surface. Figure 11(a) shows the baseline flow field, that is, with no passage vortices. Figure 11(b) shows the generic starting flow field where a set of passage vortices have been incorporated in the core flow field. These passage vortices are in the region between the plug surface and the lower part of the lobe wall as described previously and shown in figures 9 and 10. The complete secondary flow field at the starting point, which is the lobe exit plane (refer to fig. 4), is shown in figure 12(a). The computational results were reflected to include two lobe and three fan regions as shown. A strong vortex pattern can be observed which is aligned with the interface region baetween the fan and core streams, as well as the small passage vortices near the plug surface. At station number 8, which is located half way along the plug, the vortex pattern begins to condense into a more circular pattern and moves radially outward. As indicated by the disappearance of radial inward flow near the plug surface the passage vortices disappear by station number 13. The main vortex pattern continues its outward movement (figs. 12(c) to (e)). At the mixer exit plane (station number 21) the vortex is still relatively strong.

A comparison between the measured and computed total temperature contours at the mixer exit plane (station number 21) is presented in figure 13. The development of the horseshoe-shaped total temperature contour first identified in reference 6 is clearly evident. This temperature signature is the result of the secondary flow field which sustains itself by the normal static pressure gradients within the mixer nozzle passage.

A comparison between the measured and computed total temperature distributions at the mixer nozzle exit are presented in figure 14 for six rake positions. The centerline of the fan flow is at a theta value of 0 and the core flow centerline is at a theta value of 15 degrees (see fig. 5). Computations were made assuming ideal inflow conditions (no secondary flow), baseline inflow conditions (secondary flow without passage vortex), and generic inflow conditions (secondary flow with passage vortex). A comparison between the calculations using the generic secondary inflow pattern and the measured data show excellent agreement. The baseline inflow conditions yielded good agreementa except over the first 20 percent of the radius. The strong influence of the secondary flow structure is evident by comparing the solid with the dashed lines which represent the generic and ideal inflow conditions. It is apparent that the characteristic horseshoe-shaped temperature signature identified in reference 6 resulted from the inflow secondary flow vortex structure established by the initial core and fan streams.

12C Mixer

The corresponding data and computations for the 12C mixer are presented in figures 15 to 17. The starting velocity vector field is shown in figure 15 and is based on an average radial velocity of 13.7 and 8 percent of the streamwise core and fan velolcities, based on the experimental measurements. Figure 15(a) shows the baseline flow field. Figure 15(b) shows the generic starting flow field wherein the passage vortices are located near the plug surface. the complete secondary flow field at the lobe exit plane is presented in figure 16(a). The subsequent changes in the flow field

downstream are shown in figures 16(b) to (e). The qualitative features of the secondary flow pattern are similar to those shown previously for the 12B mixer. However, the magnitude of the radial flows is smaller and results in less radial displacement of the main vortices.

A comparison of the measured and computed total temperature distributions at the mixer nozzle exit are shown in figure 17 for six angular locations. In this comparison it is seen that the baseline inflow condition as well as the ideal inflow condition yield poor agreement with the experimental data, whereas the generic condition leads to excellent agreement. It is noted that the 12C mixer yields a radial temperature distribution distinctly different from that shown for the 12B in figure 14.

12A Mixer

Radial temperature distributions at the mixer exit plane for the 12A mixer are shown in figure 18. As with the previous two geometries, the generic inflow condition yields the best agreement with the data. The analysis appears to mess the spread of secondary flow and to interpredict temperature mixing oiver the inner 10 percent of the radius and overpredicts near the 60-percent point based on all the data points. However, it is noted that the two experimental data sets have significant scatter at the 60-percent radial position.

B. Influence of Hot Core Temperature

The results presented in the previous section were based on the warm flow testing where the ratio of fan-to-core strean total temperature was 0.740. In this section, the results from a fully simulated or hot flow condition with a temperature ratio of 0.40 are presented.

Computations were made using the generic, baseline, and ideal inflow conditions for the 12B mixer having a high temperature primary stream. The ratio of core-to-fan total temperature of 0.40 matched the experimental values used in the test program. The secondary velocity vector field was constructed using the same average radial flows as used in the previous calculations (fig. 14). The primary velocity was increased assuming matched Mach numbers and total pressures in the two streams at the lobe exit plane. A comparison of the computed results with the experimental data is shown in figure 19. The comparison is at the mixer exit plane, that is, station number 21, and includes six angular locations from the centerline of the fan flow, theta = 0, to the centerline of the core flow, theta = 15. As in the previous comparions, the generic inflow condition yields the poorest agreement. It is noted that the experimental data at the fan centerbody (fig. 19(a)) shows a small temperatuare rise at a normalized radius of 0.7, which was not present in the warm flow testing (see fig., 14(a)). This rise indicates spreading of the primary stream into the core of the fan stream. The computer code underpredicted either the secondary flows or the temperature mixing in this region.

C. Influence of Turbulence

Additional computations were performed with a higher level of free-stream turbulence in both the fan and core streams for the 12B mixer geometry. The computations were made for only the generic inflow condition. The construction of the starting secondary flow field was identical to that de-

scribed in section A. The temperature ratio, T_F/T_F, used in the computations was 0.40. The turbulence intensity (fluctuating component of the mainstream velocity/mean streamwise velocity) was increased to 12 percent and the result is shown in figure 20. Also shown in figure 20 is the previous generic result for a turbulence intensity of 4 percent (from fig. 19). The experimental data are also from the previous figure. No attempt was made to run the experimental test with higher turbulence. The results in figure 20 show that the higher intensity (dashed lines) lead to greater temperature mixing near the shroud, that is, normalized radius of about 0.85, over the theta range of 6 to 15 degrees (figs. 20(c) to (f)). At the same radial position, no additional mixing is predicted with the higher intensity near the fan lobe centerline (figs. 20(a) and (b)). A slight shift is observed in the radial position of the maximum temperature, as seen in figures 20(d) to (f). The higher turbulence intensity moves the peak to a lower radial position.

At the intermediate radial positions, the larger intensity value yields temperature ratios which are closer to the ideally mixed value of 0.5. And finally, at the lower radial locations (~0.2), the difference in temperature ratio results from the two intensities begin to approach zero.

CONCLUDING REMARKS

A finite difference procedure has been used to compute the mixing for three different lobe geometries which were experimentally tested. The following conclusions were made based on a comparison of the analyses and the data:

1. The dominant mechanisms within modern turbofan forced mixers is associated with the pressure driven secondary flows arising within the lobe region upstream of the mixer and their development in the mixing region.

2. Secondary flow generation at the lobe exit is caused by three principle mechanisms, that is, vorticity due to turning (flap vorticity), passage vorticity, and horseshoe vorticity.

3. The flap and passage vorticity appear to be adequate flow mechanisms in initial flow conditions to obtain good agreement with experimental mixer exit profiles.

4. A generic representation of the vorticity mechanisms yield good agreement between analyses and experiments for three different lobe geometries and for two different temperature ratios of operation.

5. There is a critical need to obtain detailed experimental information regarding the nature of the secondary flows generated within the lobe region in order to properly analyze mixer nozzle. Empirical data relating lobe geometry effects on secondary flow generation is highly desirable as a design standpoint.

REFERENCES

1. Kuchar, A. P. and Chamberlin, R., "Scale Model Performance Test Investigation of Exhaust System Mixers for an Energy Efficient Engine (E^3) Propulsion System," AIAA Paper 80-0229, Jan. 1980.
2. Shumpert, P. K., "An Experimental Model Investigation of Turbofan Engine Internal Exhaust Gas Mixer Configurations," AIAA Paper 80-0228, Jan. 1980.

3. Kozlowski, H. and Kraft, G., "Experimental Evaluation of Exhaust Mixers for an Energy Efficient Engine," AIAA Paper 80-1088, June 1980.
4. Birch, S. F., Paynter, G. C., Spalding, D. B., and Tatchell, D. G., "Numerical Modeling of Three-Dimensional Flows in Turbofan Engine Exhaust Nozzles," Journal of Aircraft, Vol. 15, Aug. 1978, pp. 489-496.
5. Bowditch, D. N., McNally, W. D., Anderson, B. H., Adamczyk, J. J., and Sockol, P. M., "Computational Fluid Mechanics of Internal Flow," Aeropropulsion 1979, NASA CP-2092, 1979, pp. 187-230.
6/ Povinelli, L. A., Anderson, B. H., and Gerstenmaier, W., "Computation of Three-Dimensional Flow in Turbofan Mixers and Comparison with Experimental Data," AIAA Paper 80-0227, Jan. 1980.
7. Kreskovsky, J. P., Briley, W. R., and McDonald H., "Development of a Method for Computing Three-Dimensional Subsonic Turbulent Flows in Turbofan Lobe Mixers," Scientific Research Associates, Inc., Glastonbury, CT., R79i-300006-F, Nov. 1979.
8. Briley, W. R.f, and McDonald, H., "Analysis and Computation of Viscous Subsonic Primary and Secondary Flows," Computational Fluid Dynamics Conference, American Institute of Aeronautics and Astronautics, Inc., 1979, AIAA Conf. Paper 79-1453, pp. 74-88.
9. Patterson, R., and Werle, M. J., "Turbofan Forced Mixer Flow Field," United Technologies Research Center, East Hartford, CT, UTRC/R79 - 912924 - 24, July 1979.
10. Anderson, B. H., Povinelli, L. A., and Gerstenmaier, W. G., "Influence of Pressure Driven Secondary Flows osn the Behavior of Turbofan Forced Mixers," AIAA Paper 80-1198, July 1980.
11. Launder, B. E., and Spalding, D. B., "The Numerical Computation of Turbulent Flows," Computer Methods in Applied Mechanics and Engineering, Vol. 3, Mar. 1974, pp. 269-289.
12. Dudzinski, T. J., and Krause, L. N., "Flow-Direction Measurement with Fixed-Position Probes," NASA TM X-1904, 1969.
13. Anderson, O. L., "Finite - Difference Solution for Turbulent Swirling Compressible Flow in Axisymmetric Ducts with Struts," NASA CR-2365, 1974.
14. Anderson, O. L., "Turbofan Forced Mixer Nozzle Internal Flowfield," NASA Contractors Report to be published, 1981.

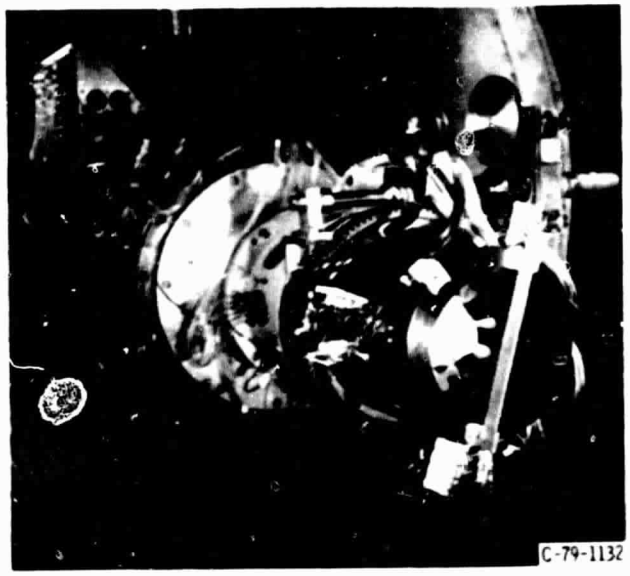

Figure 1. - Experimental mixer nozzle.

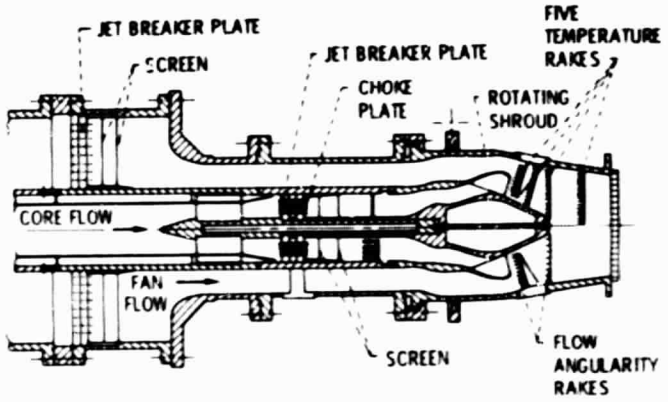

(a) MIXER NOZZLE CROSS-SECTION

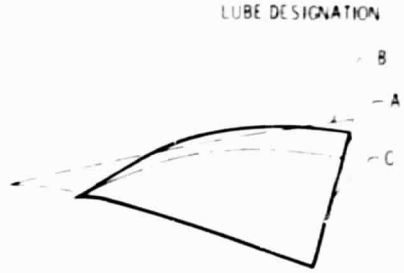

(b) LOBE GEOMETRY, LONGITUDINAL CONTOURS.

Figure 2. - Mixer geometry.

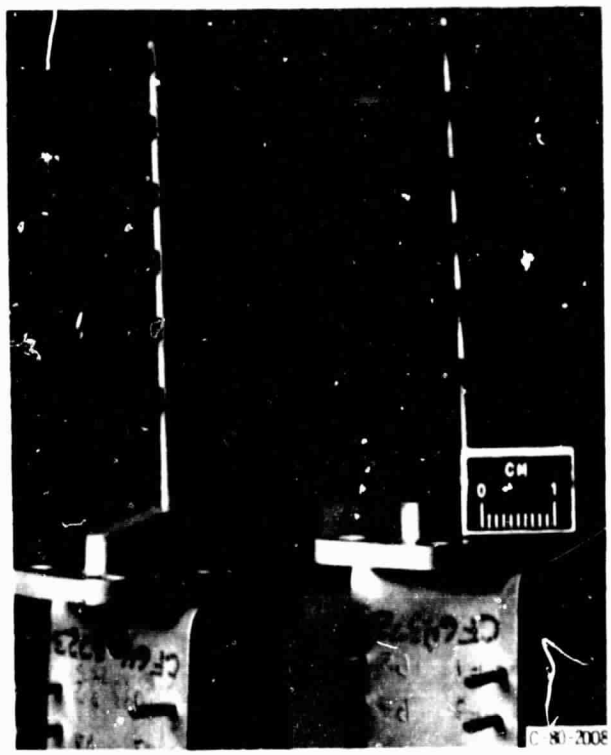

Figure 3. - Flow angularity rates.

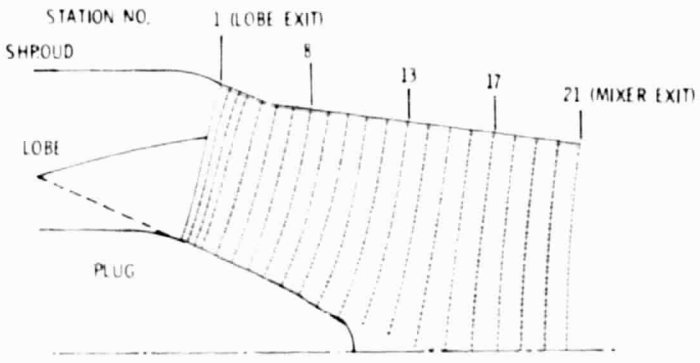

Figure 4. - Mixer nozzle computational mesh.

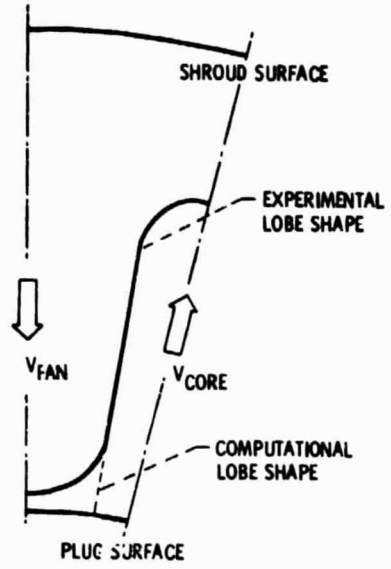

Figure 5. - Transverse computational segment.

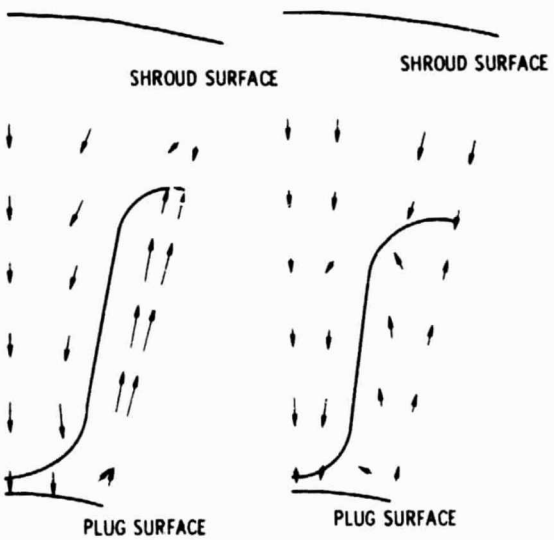

Figure 6. - Measured secondary velocity vectors, lobe exit station.

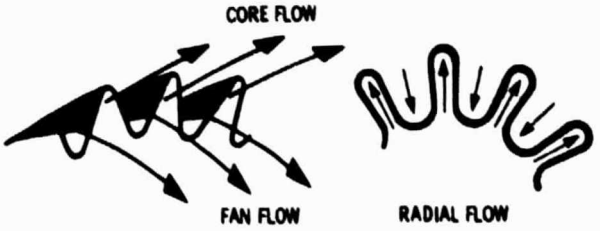

(a) BASIC FLOW TURNING. (b) RADIAL FLOW ORIENTATION.

Figure 7. - Secondary flow generation, turning (flap) vorticity.

(a) FAN PASSAGE.

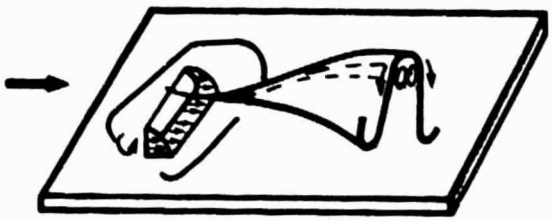

(b) CORE PASSAGE.

Figure 8. - Secondary flow generation, horseshoe vortex.

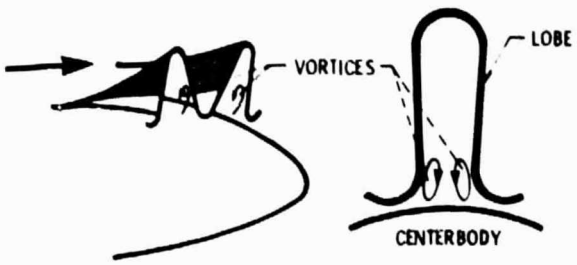

Figure 9. - Secondary flow generation, passage vortex.

Figure 10. - Tuft behavior in core flow.

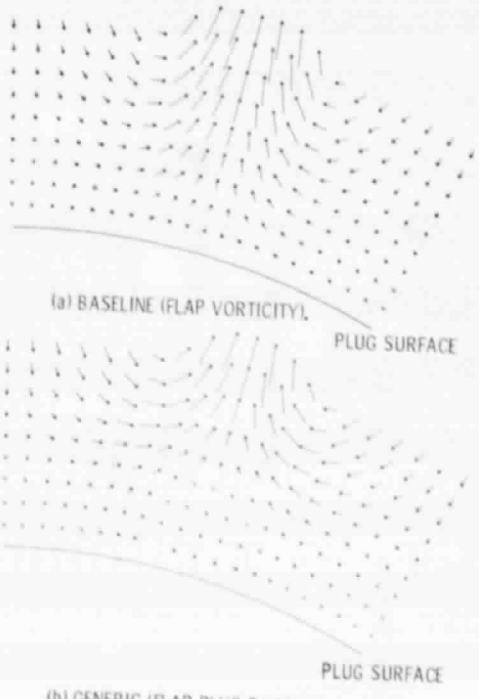

(a) BASELINE (FLAP VORTICITY).

(b) GENERIC (FLAP PLUS PASSAGE VORTICITY).

Figure 11. - Initial secondary flow field, lobe exit plane, 12B Mixer, $T_C/T_F = 0.74$.

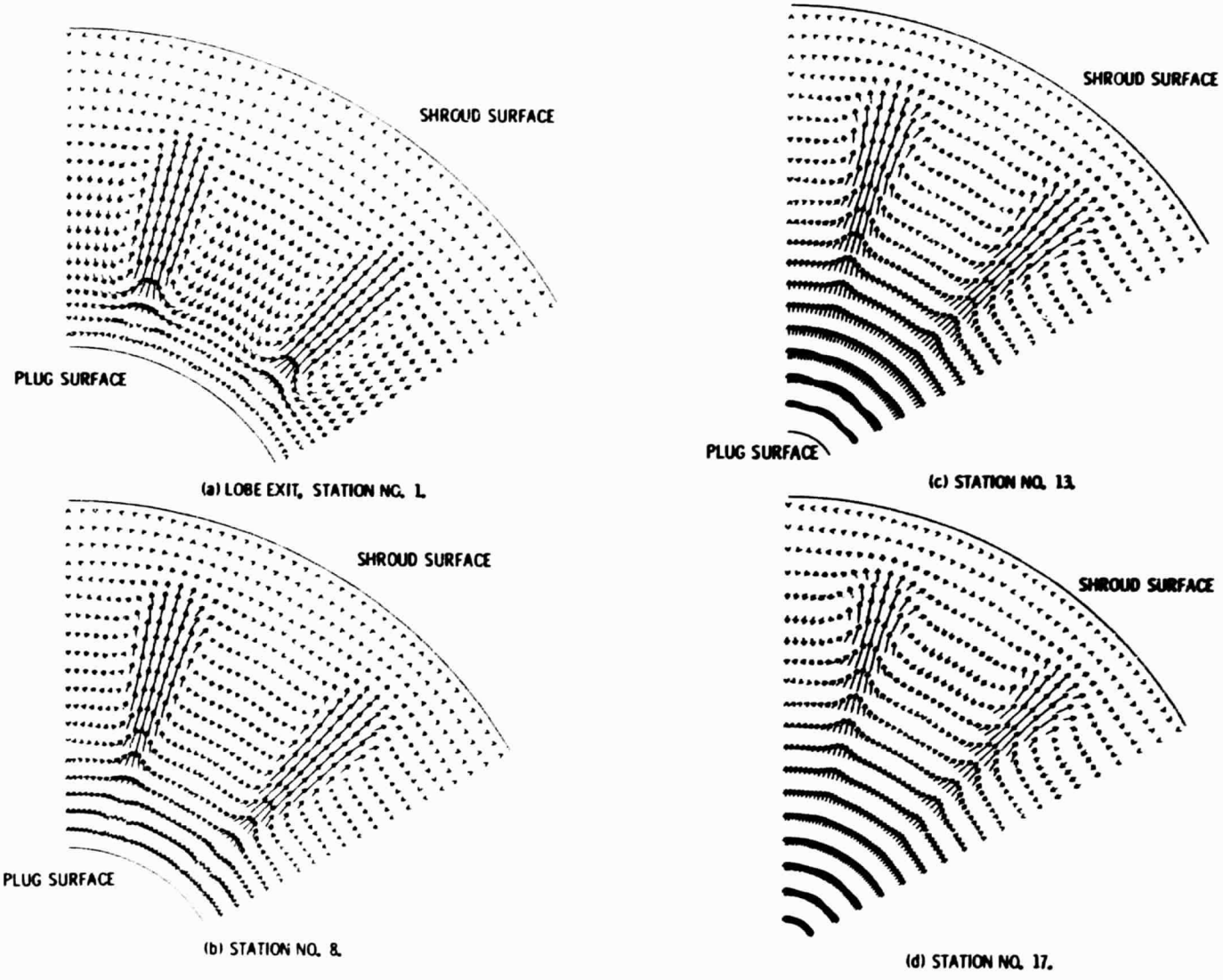

Figure 12. - Computed secondary velocity vectors.

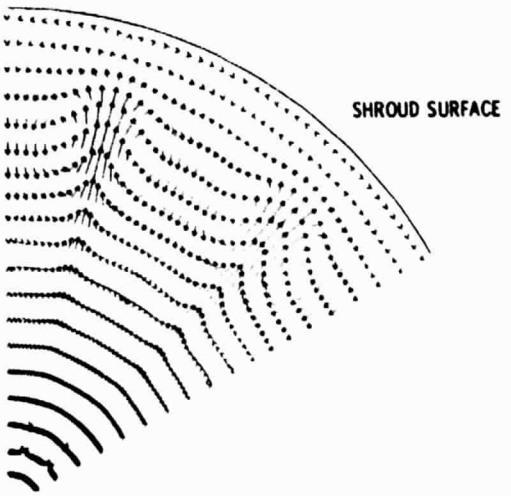

(e) MIXER EXIT, STATION NO. 21.

Figure 12. - Concluded.

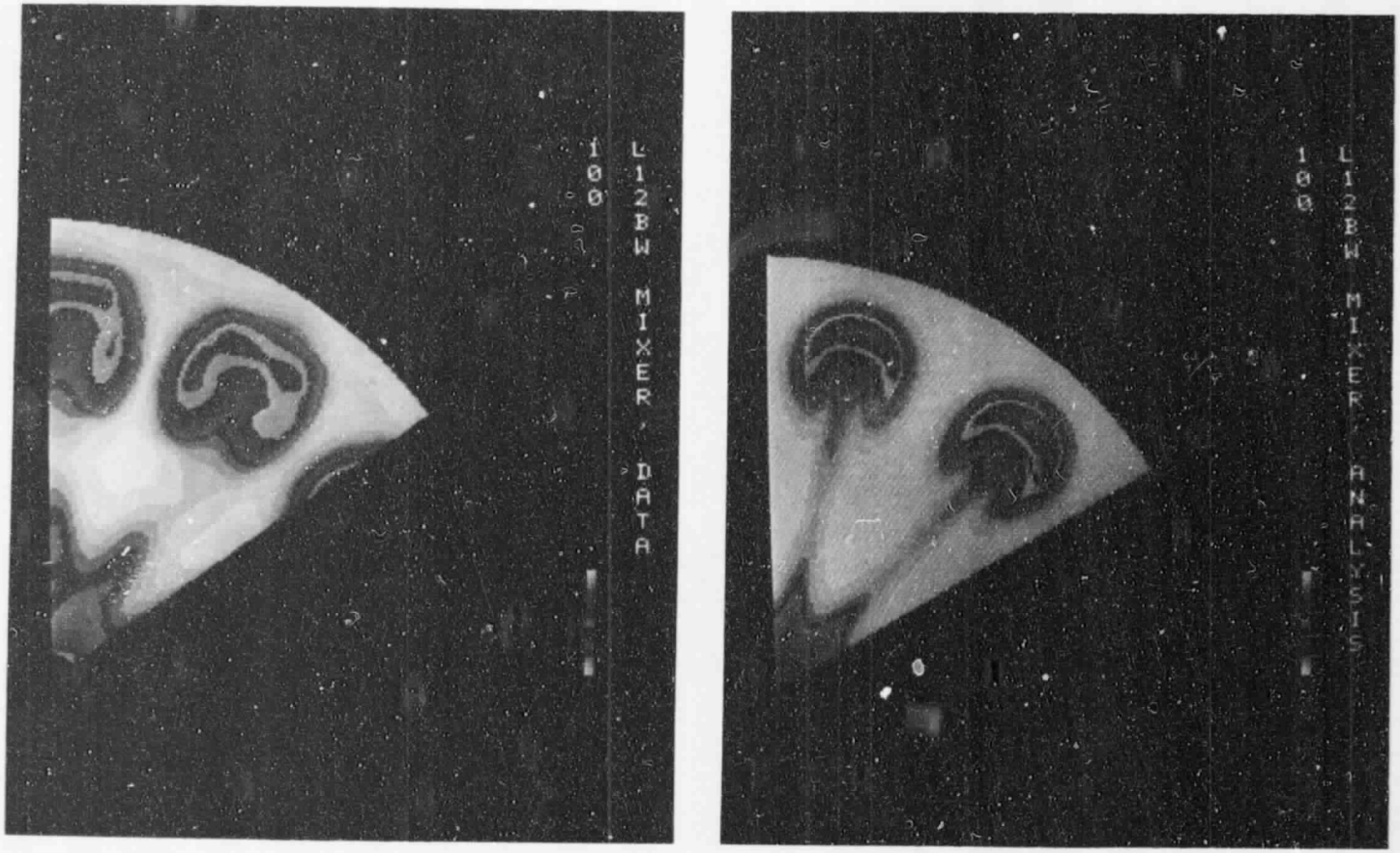

(a) EXPERIMENT

(b) ANALYSIS

Figure 13. - Comparison of total temperature contours at mixer exit plane.

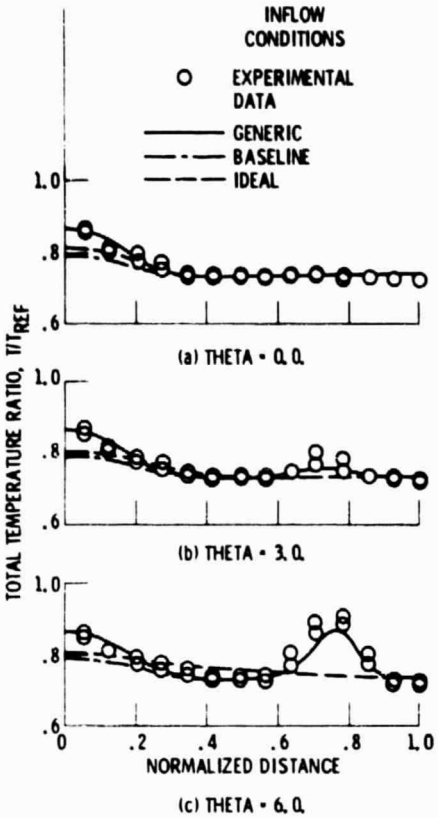

Figure 14. - Comparison of computed temperature profiles with experimental data 12B Mixer, $T_F/T_C = 0.74$, Station 21.

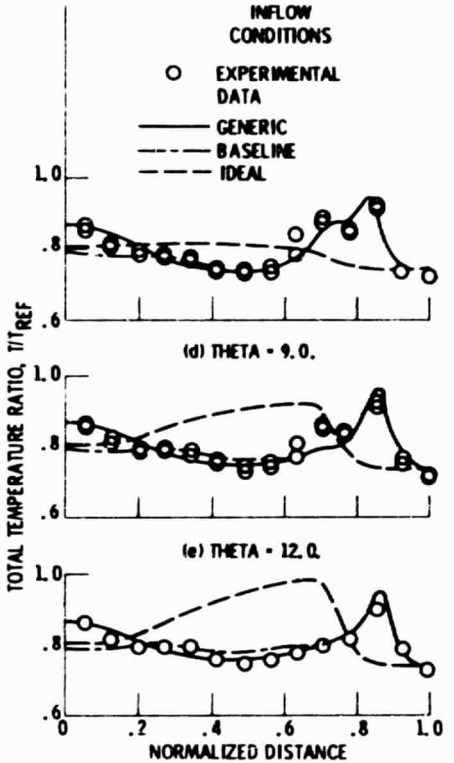

Figure 14. - Concluded.

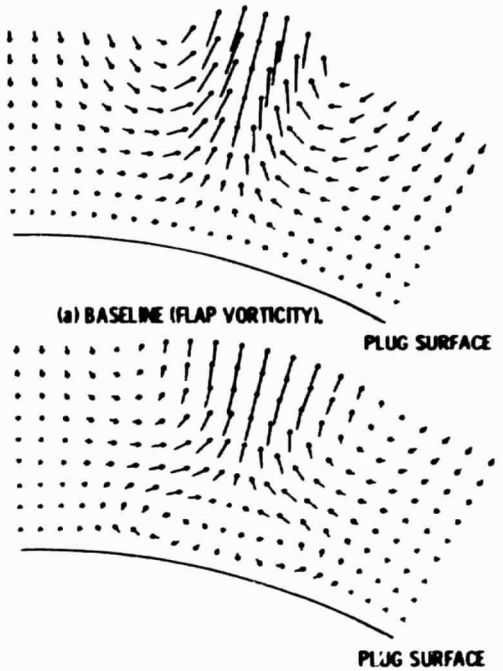

Figure 15. - Initial secondary flow field, lobe exit plane, 12 C Mixer, $T_F/T_C = 0.74$.

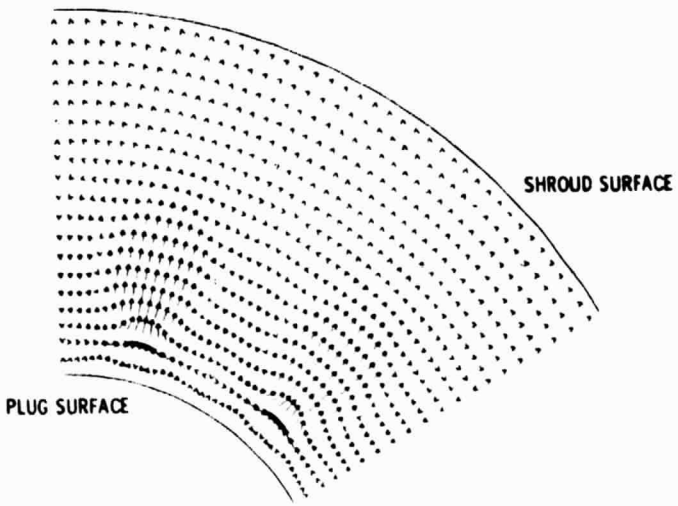

(a) LOBE EXIT, STATION NO. 1.

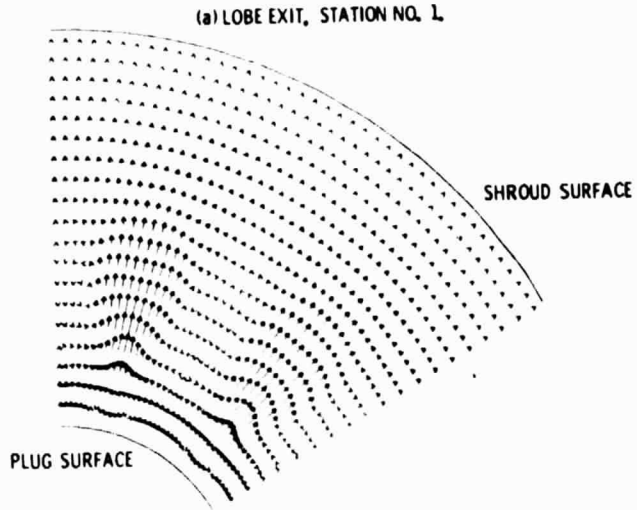

(b) STATION NO. 8

Figure 16. - Computed secondary velocity vectors.

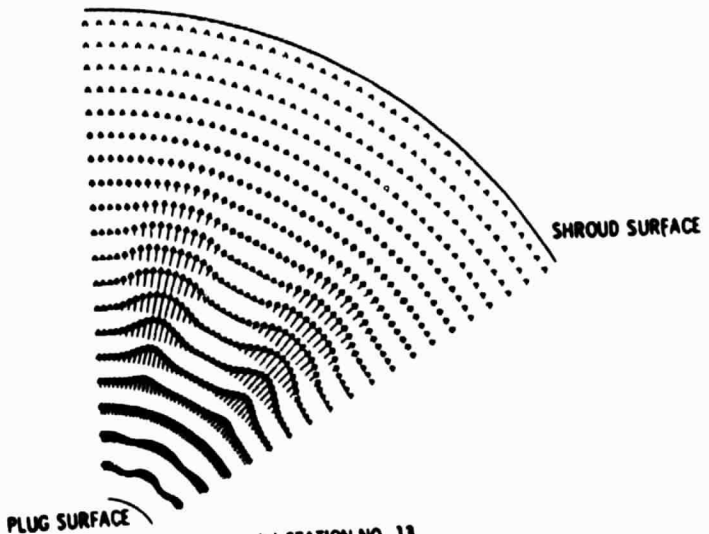

(c) STATION NO. 13.

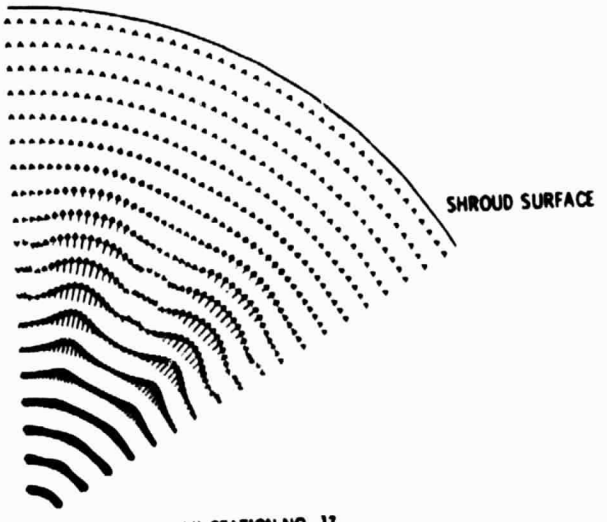

(d) STATION NO. 17.

Figure 16. - Continued.

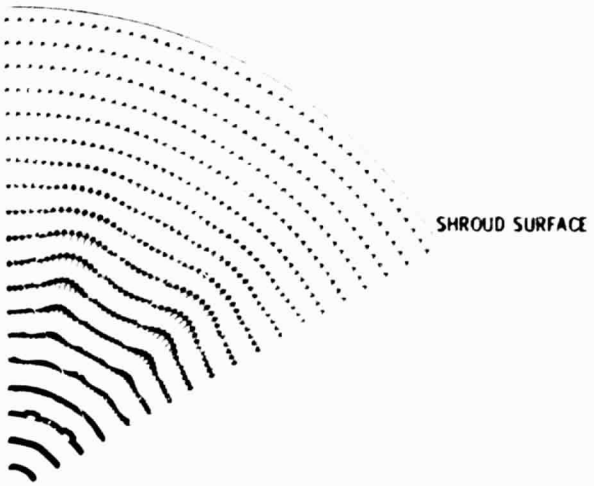

(c) MIXER EXIT, STATION NO. 21.

Figure 16. - Concluded.

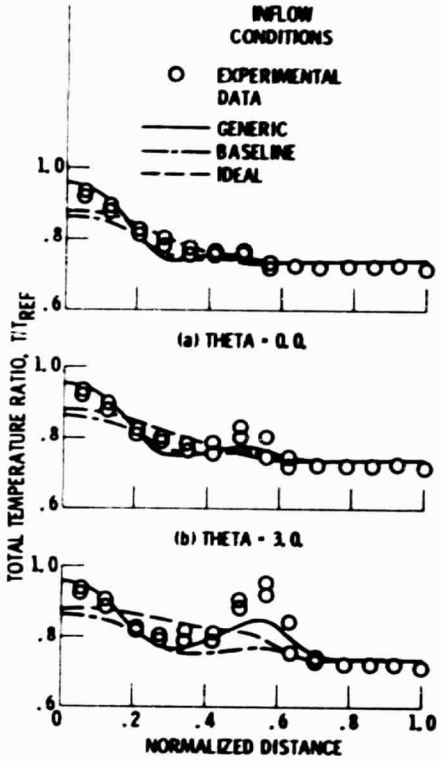

Figure 17. - Comparison of computed temperature profiles with experimental data. 12C Mixer, T_F/T_C = 0.74, Station 21.

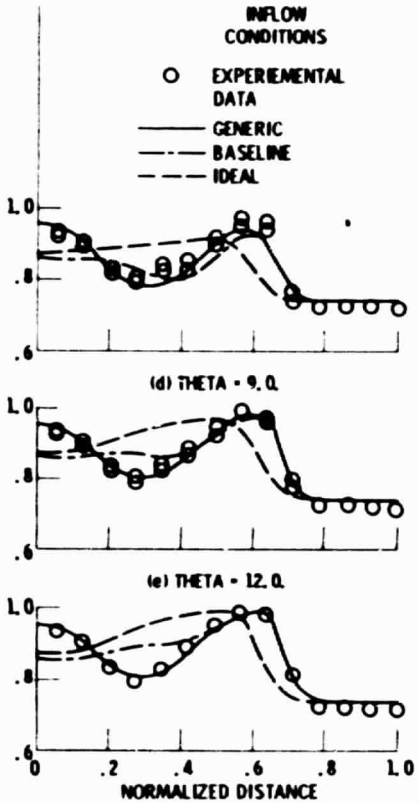

Figure 17. - Concluded.

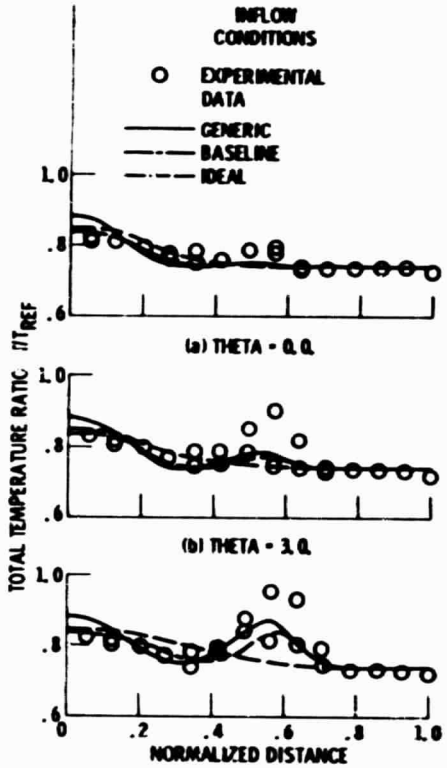

Figure 18. - Comparison of computed and experimental temperature profiles. 12A Mixer, $T_F/T_C = 0.74$.

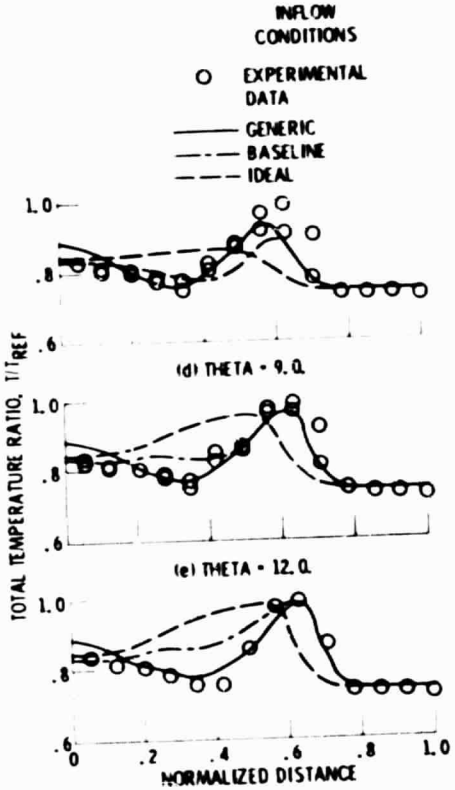

Figure 18. - Concluded.

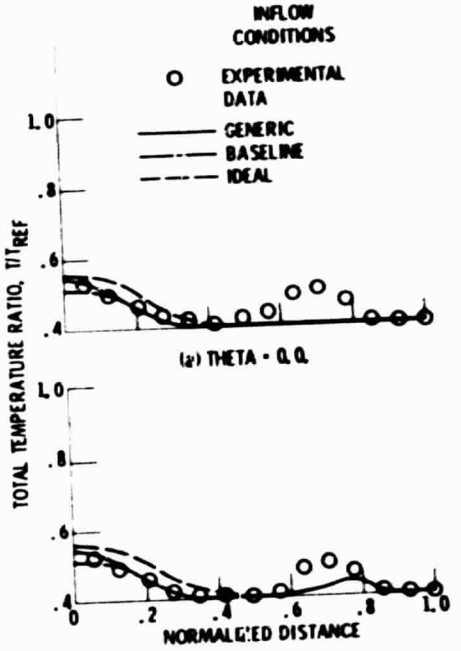

Figure 19. - Comparison of computed and experimental temperature profiles. 12B Mixer, T_p/T_c = 0.40.

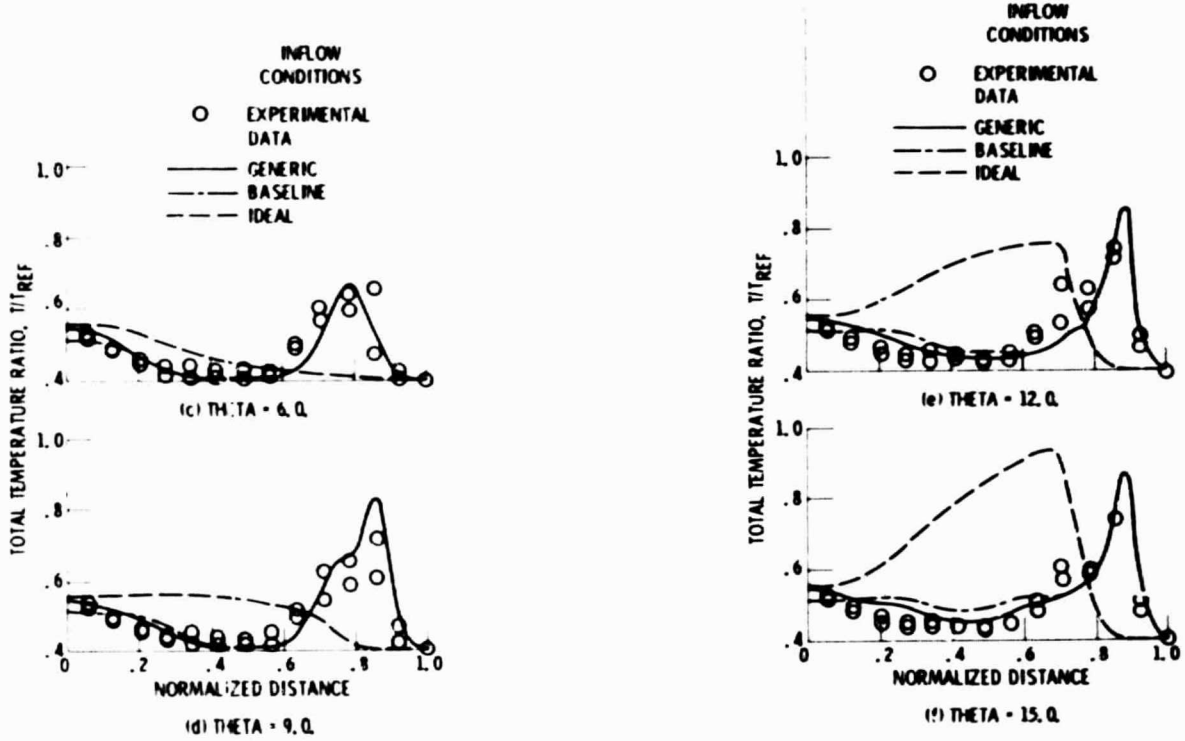

Figure 19. - Concluded.

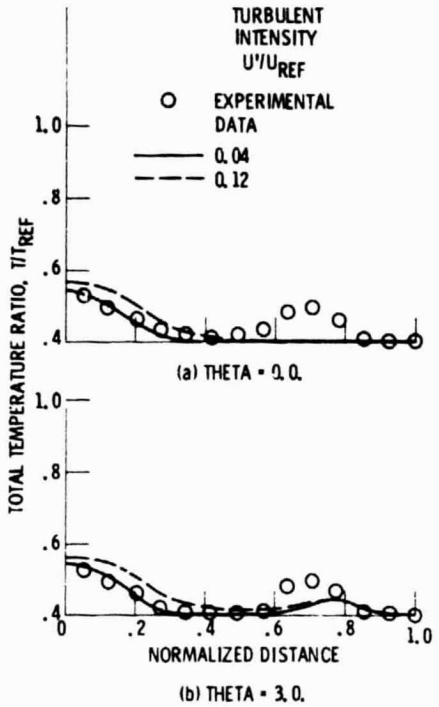

Figure 20. - Comparison of computed and experimental temperature profiles. 12B Mixer, $T_F/T_C = 0.40$.

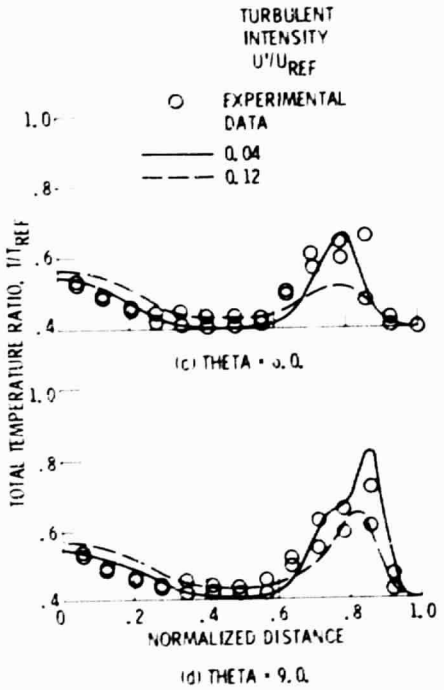

(c) THETA = 6.0

(d) THETA = 9.0

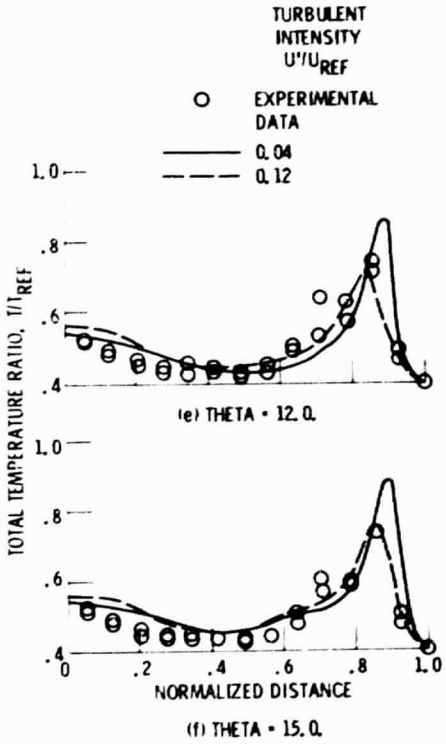

(e) THETA = 12.0

(f) THETA = 15.0

Figure 20. - Concluded.